*magnetochemistry*

MDPI

*Article*

# A Heptacobalt(II/III) Dicubane Cluster with Polyoxometalate and Acetato Ligands: Synthesis, Crystal Structure, and Magnetic Properties †

**Gonzalo Abellán-Dumont [1], Juan Modesto Clemente-Juan [2,*] and Carlos Giménez-Saiz [1,*]**

[1] Departament de Química Inorgánica, Universitat de València, Dr Moliner 50, 46100 Burjassot, Spain; gonzalo.abellan-dumont@uv.es
[2] Instituto de Ciencia Molecular (ICMol), Universitat de València, 46980 València, Spain
* Correspondence: juan.m.clemente@uv.es (J.M.C.-J.); carlos.gimenez@uv.es (C.G.-S.)
† This contribution is dedicated to the outstanding scientific careers of Miguel Julve and Paco Lloret, a great source of inspiration, both scientifically and personally, for their colleagues at the Inorganic Chemistry Department of the University of Valencia. Sadly, Miguel recently passed away. We will miss his friendship and scientific collaboration.

**Abstract:** The new polyoxometalate $[Co_7(OH)_6(H_2O)_2(CH_3COO)_4(PW_9O_{34})_2]^{13-}$ (**1**) has been synthesized and characterized by IR, UV-Vis-NIR, TGA-TDA, X-ray single crystal analysis, and magnetic studies; **1** consists of two trilacunary heptadentate B-α-$[PW_9O_{34}]^{9-}$ ligands encapsulating a heptacobalt dicubane-like $\{Co^{II}_6Co^{III}O_8\}$ core, in which the $Co^{2+}$ ions are further coordinated by two water molecules and four acetate anions acting as monodentate ligands. The magnetic properties of **1** have been fitted according to an anisotropic exchange model in the low-temperature regime and discussed on the basis of ferromagnetic interactions between $Co^{2+}$ ions with angles Co–L–Co (L = O, OH) close to orthogonality and weakly antiferromagnetic interactions between $Co^{2+}$ ions connected through a central diamagnetic $Co^{3+}$ ion.

**Keywords:** polyoxometalate; cobalt cluster; magnetic properties; acetate ligands; ligand substitution; crystal structure; anisotropic exchange; spin–orbit coupling

check for updates

Academic Editor: Marius Andruh

Received: 18 May 2025
Accepted: 26 May 2025
Published: 3 June 2025

**Citation:** Abellán-Dumont, G.; Clemente-Juan, J.M.; Giménez-Saiz, C. A Heptacobalt(II/III) Dicubane Cluster with Polyoxometalate and Acetato Ligands: Synthesis, Crystal Structure, and Magnetic Properties. *Magnetochemistry* **2025**, *11*, 48. https://doi.org/10.3390/magnetochemistry11060048

**Copyright:** © 2025 by the authors. Licensee MDPI, Basel, Switzerland. This article is an open access article distributed under the terms and conditions of the Creative Commons Attribution (CC BY) license (https://creativecommons.org/licenses/by/4.0/).

## 1. Introduction

Polyoxometalates (POMs) are discrete, anionic metal–oxo clusters containing early *d*-block metals such as W, Mo, or V in their highest oxidation states [1,2]. These metals form $MO_6$ octahedra, which share corners and/or edges while keeping one or more terminal M=O bonds, avoiding the formation of infinite solid-state compounds. Other metal or non-metal containing polyhedra (e.g., $PO_4$, $SiO_4$) can also be combined with the constituent $MO_6$ building blocks, giving rise to an enormous structural variety of POMs. The most prototypical POM structures are the Keggin (e.g., $[PW_{12}O_{40}]^{3-}$) and the Dawson (e.g., $[P_2W_{18}O_{62}]^{6-}$) anions, in which one or more $WO_6$ octahedra can be removed by controlled hydrolysis producing lacunary derivatives that are capable of acting as polydentate ligands of almost any kind of 3*d* or 4*f* metal. This fact, together with their ability to be covalently functionalized with organic components [3], combined with metal–organic frameworks [4], or accept electrons [5], allows POMs to have applications in many fields, such as catalysis [3,4,6,7], medicine [8,9], material science [10,11], sensor science [12,13], or magnetism.

In molecular magnetism, POMs play an important role because they allow the assembly of large magnetic clusters encapsulated by bulky diamagnetic POM ligands that

assure the effective insulation of the magnetic cores and, therefore, avoid intermolecular magnetic interactions. Given this key feature, the usefulness of the effective Hamiltonians in magnetic clusters of high nuclearities and high symmetry has been examined [14], and POMs with single-molecule magnet behavior based on 3*d* or 4*f* metal ions have been obtained [15,16]. In addition, the ability of POMs to be reduced by a variable number of electrons has been used to study the exchange and transfer interaction in mixed-valence POM systems (heteropolyblues) [17].

Cobalt-containing POMs represent an excellent opportunity to conduct detailed studies on the magnetic exchange interactions in multicobalt clusters. The $Co^{2+}$ ion ($d^7$) exhibits a high spin S = 3/2, when octahedrally coordinated by POM ligands, and an unquenched orbital momentum. However, the extensive splitting of the $^4T_{2g}$ ground term, due to the first-order spin–orbit coupling and the octahedral distortion, leads to an effective ground spin doublet (S = ½), which has a large anisotropy [18]. Insights in the anisotropic nature of the exchange interactions in $Co^{2+}$ clusters have been provided by inelastic neutron scattering (INS) studies on several POMs containing ferromagnetically coupled $Co^{2+}$ clusters, i.e., $[Co_4(H_2O)_2(PW_9O_{34})_2]^{10-}$, $[Co_3W(H_2O)_2(ZnW_9O_{34})_2]^{12-}$, and $[Co_3Na(H_2O)_2(P_2W_{15}O_{62})_2]^{17-}$ [19]. This knowledge has been applied to characterize the magnetic interactions in other POMs containing $Co^{2+}$ clusters with different topologies and coexisting ferromagnetic and antiferromagnetic interactions [20]. In particular, we have reported a series of POM compounds containing isolated dicubane $\{Co_7O_8\}$ cobalt clusters [21] and Keggin (B-α-$[PW_9O_{34}]^{9-}$) or Dawson (α-$[P_2W_{15}O_{56}]^{9-}$) trilacunary ligands, namely, $[Co_7(OH)_6(H_2O)_6(PW_9O_{34})_2]^{9-}$ (**2**), $[Co_7(OH)_6(H_2O)_4(PW_9O_{34})_2]_n^{9n-}$ (**3**), and $[Co_7(OH)_6(H_2O)_6(P_2W_{15}O_{62})_2]^{15-}$ (**4**) (see Figure 1). All these dicubane clusters contain six $Co^{2+}$ ions arranged in two triads separated by one central $Co^{3+}$ ion and represent rare examples of cobalt clusters encapsulated by POMs having cobalt in both oxidation states (see Figure 1, left). These compounds still remain the only examples of POMs containing heptanuclear cobalt clusters with a dicubane topology, although examples of this topology with nickel and manganese do exist in $[Ni_7(OH)_6(H_2O)_6(P_2W_{15}O_{56})_2]^{16-}$ [22], $[Ni_7(H_2O)_4(OH)_6(SiW_8O_{31})_2]^{12-}$ [23], and $[Mn_7O_6(H_2O)_6(P_2W_{15}O_{56})_2]^{14-}$ [24].

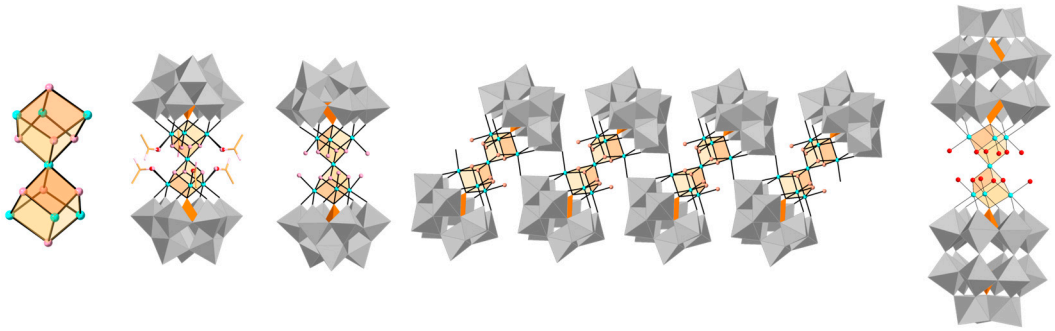


**Figure 1.** Heptacobalt dicubane $\{Co^{II}_6Co^{III}O_8\}$ cluster (left) encapsulated in POMs **1**–**4**. POM **1**, described in this work for the first time, has two water molecules and four acetate anions coordinating the six $Co^{2+}$ ions of the cluster. POMs **2**–**4** are previously reported members of this series. The formulas of **1**–**4** are mentioned in the main text.

Here we report on the synthesis, IR and UV-Vis-NIR spectra, thermogravimetric and differential thermal analysis, crystal structure, and magnetic properties of a new POM containing a heptacobalt dicubane cluster, in which four of the six water molecules that coordinate the $Co^{2+}$ ions in the previously reported POM **2** have been substituted by acetate anions that act as monovalent ligands: $[Co_7(OH)_6(H_2O)_2(CH_3COO)_4(PW_9O_{34})_2]^{13-}$ (**1**).

## 2. Materials and Methods

### *2.1. Materials*

All reagents were of high-purity grade quality, obtained from commercial sources, and used without further purification. Pure water (ρ > 18 MΩ·cm) was used throughout. Reactions were performed in conventional round-bottomed flasks heated using a Heidolph magnetic hotplate stirrer fitted with aluminum alloy heating blocks suitable for round-bottom flasks. The temperature was controlled using a Pt-1000 sensor (Heidolph, Schwabach, Germany) connected to the hotplate.

### *2.2. Physical Techniques*

IR spectra were recorded on an Agilent Cary 630 FTIR spectrometer (Agilent, Santa Clara, CA, USA) with diamond ATR sampling. Microanalysis of W, Co, P, and Na was carried out by energy-dispersive X-ray spectroscopy (EDX) using a SCIOS 2 field emission scanning electron microscope coupled with a microanalysis detector, Oxford Ultim Max 170. Carbon and hydrogen contents were determined using a FlashSmart elemental analyzer from Thermo Fisher Scientific (Waltham, MA, USA), both from the Central Support Service for Experimental Research of the University of Valencia (SCSIE). TGA/TDA measurements were carried out with a TA Instruments TGA550 (New Castle, DE, USA), heating from room temperature to 680 °C in a dry air atmosphere, using the Hi-Res mode, in which the heating rate varies depending on the mass loss of the sample. Diffuse reflectance spectra were registered on a Cary 4000 Spectrophotometer (Agilent), using $BaSO_4$ as reference.

### *2.3. Single-Crystal X-Ray Diffraction*

A suitable crystal of $Na_{13}$-**1**·$37H_2O$, obtained as described in the synthesis section, was coated with Paratone-N oil, suspended on a small fiber loop, and placed in a stream of cooled nitrogen (150 K) on a Bruker APEX-II CCD diffractometer equipped with a graphite-monochromated (Mo) X-ray Source (λ = 0.71073 Å). The data collection routines, unit cell refinements, and data processing were carried out using the APEX3 v2017.3-0 software package [25], and structure solution and refinement were carried out using SHELXT 2018/2 and SHELXL-2019/2 [26]. A multi-scan absorption correction was applied. The solution and refinement of the structure reveal that the terminal ligands of the six $Co^{2+}$ ions (Co2 and Co3) of the heptanuclear {$Co_7O_8$} cluster correspond to four acetate anions and two water molecules, which are statistically disordered over the six positions occupied by the terminal ligands. Each of the two crystallographically independent acetate ligands is also disordered in several components that share the coordinating oxygen atom. EXYZ and EADP constraints commands were used to equate the xyz coordinates and Uij thermal parameters of O23a and O23b (the coordinating oxygen atoms of the disordered components of the first acetate ligand) and of O25a and O25b (belonging to the second acetate). Therefore, the refinement of acetate and water ligands involved partial occupancies, and appropriate similarity and local geometry restraints (SAME and FLAT commands). The components of their anisotropic displacement parameters were also restrained using a combination of hard and soft restraints (DELU and SIMU). The solvent/cation region of the structure also presents a high degree of disorder, as is commonly found in most crystal structures of large polyoxometalates. Therefore, some of the cations (Na4) and solvent water molecules were refined using partial occupancies, and their anisotropic components were restrained to have approximate isotropic behavior using the ISOR command. Even so, the disorder in this region could not be treated completely, and some large residual densities remain near the sodium cations and water molecules. H atoms on carbon atoms were included at calculated positions and refined with a riding model with relative isotropic displacement parameters. H atoms of water molecules or hydroxyl anions were not located.

All non-H atoms were refined anisotropically. Crystal data and details of the data collection and refinement for $Na_{13}$-**1**·$37H_2O$ are listed in Table 1. CCDC 2419765 contains the supplementary crystallographic data for $Na_{13}$-**1**·$37H_2O$. These data are provided free of charge by the Cambridge Crystallographic Data Centre.

**Table 1.** Summary of the crystal data and refinement details for $Na_{13}[Co_7(OH)_6(H_2O)_2(CH_3COO)_4(PW_9O_{34})_2]$ ·$37H_2O$ ($Na_{13}$-**1**·$37H_2O$).

| **Formula** | **$C_8H_{96}Co_7Na_{13}O_{121}P_2W_{18}$** |
|---|---|
| $M_r$ (g/mol) | 6211.46 |
| Crystal system | Orthorhombic |
| Space group | *Cmca* (No. 64) |
| $T$ (K) | 150 (2) |
| $\lambda$ (Å) | 0.71073 |
| $a$ (Å) | 22.2275 (8) |
| $b$ (Å) | 20.0193 (8) |
| $c$ (Å) | 29.0406 (11) |
| $\alpha$ (deg) | 90 |
| $\beta$ (deg) | 90 |
| $\gamma$ (deg) | 90 |
| $V$ (Å$^3$) | 12,922.5 (9) |
| $Z$ | 4 |
| $\rho$ (mg/m$^3$) | 3.193 |
| $\mu$ (Mo K$\alpha$) (mm$^{-1}$) | 17.002 |
| $F$(000) | 11,224 |
| Crystal size (mm) | 0.063 × 0.179 × 0.199 |
| $\theta$ range (deg) | 2.308–39.681 |
| Index ranges for $h$, $k$, $l$ | −38/31, −35/34, −52/51 |
| Reflns. with I > 2σ($I$) | 16,291 |
| Independent reflns. | 18,871 |
| $R_{int}$ | 0.0527 |
| GOF on $F^2$ | 1.074 |
| Reflns. collected | 244,378 |
| Data/restraints/parameters | 18,871/328/551 |
| $R_1$, $wR_2$ [$I > 2\sigma(I)$] [a] | 0.0384, 0.0481 |
| $R_1$, $wR_2$ (all data) [a] | 0.0977, 0.1040 |
| Largest diff. peak/hole (e Å$^{-3}$) | 5.216/−6.043 |

[a] $R_1 = \sum(|F_0| - |F_c|)/\sum|F_0|$; $wR_2 = \sum[w(F_0^2 - F_c^2)^2]/\sum[w(F_0^2)^2]^{1/2}$; $w = 1/[\sigma^2(F_0^2) + (0.0431P)^2 + 308.57P]$, where $P = (F_0^2 + 2F_c^2)/3$.

### *2.4. Powder X-Ray Diffraction (PXRD)*

PXRD measurements of compound **1** were collected on a D8 ADVANCE A25 CONTROLLER powder diffractometer from Bruker AXS using Cu K$\alpha$ radiation (λ = 1.54056 Å) at room temperature and in a 2$\theta$ range from 2 to 40°. Simulated diffractograms were obtained from single-crystal X-ray data using the Mercury 2024.1.0 software from the CCDC.

### *2.5. Synthesis of $Na_{13}[Co_7(OH)_6(H_2O)_2(CH_3COO)_4(PW_9O_{34})_2]$·$37H_2O$ ($Na_{13}$-**1**·$37H_2O$)*

2.050 g (25 mmol) of $CH_3COONa$ and 1.012 g (3.6 mmol) of $CoSO_4$·$7H_2O$ were dissolved in 50 mL of water using a 100 mL round-bottomed flask. The resulting aqueous solution had a pH of ~7.9. Then, 2.42 g (1 mmol) of solid $Na_8H[PW_9O_{34}]$ (synthesized according to a literature method [27]) were added in small portions to the previous solution over a period of 15 min, with vigorous stirring. When the addition was completed, the stirring was continued for 10 min, and then, 0.072 g (0.3 mmol) of solid $Na_2S_2O_8$ was also added. After this, the round-bottomed flask was covered with a watch glass, the suspension heated to 80 °C for 2 h, and then allowed to cool back to room temperature. The resulting red-violet

solution was transferred to a flat-bottomed crystallizing dish, and the solvent was allowed to evaporate at room temperature. After 8 days of standing in this open container, orange-pink crystals of **1** were obtained, collected by filtration, washed with a small amount of cold water, and air-dried (yield: 0.521 g; 17% based on B-α-$[PW_9O_{34}]^{9-}$). Elemental ratio Na–P–W–Co calculated for $Na_{13}[Co_7(OH)_6(H_2O)_2(CH_3COO)_4(PW_9O_{34})_2]\cdot 37H_2O$ (**1**): 6.5:1:9:3.5; found by EDX: 6.5:1:8.5:3.5. Anal. calculated for carbon and hydrogen: C, 1.55%; H, 1.56%. Found: C, 1.56%; H, 1.55%.

### *2.6. Magnetic Measurements*

A crystalline sample of **1** was ground, and the powder was compacted to be used in the magnetic measurements. Variable-temperature susceptibility measurements were performed in the temperature range 2−300 K on a magnetometer equipped with a SQUID sensor (Quantum Design MPMS-XL-5, San Diego, CA, USA). The data were corrected for the diamagnetic contribution of the polyoxoanion using Pascal's constant tables. Isothermal magnetization measurements at 2 and 5 K were carried out up to a field of 7 T using the same equipment.

## 3. Results

### *3.1. Synthesis*

The synthetic procedure leading to POMs encapsulating dicubane $\{Co_7O_8\}$ clusters has been previously reported by us [21]. Two approaches can be followed: (i) the direct reaction of $Co^{2+}$ ions with a previously prepared trilacunary ligand (B-α-$[PW_9O_{34}]^{9-}$ or α-$[P_2W_{15}O_{56}]^{12-}$), or (ii) the one-pot condensation of $WO_4^{2-}$, $PO_4^{3-}$, and $Co^{2+}$ ions. Both approaches require the appropriate conditions of temperature and pH, and also the use of $S_2O_8^{2-}$ as oxidant, and have led to three different POM compounds containing the heptacobalt cluster: $[Co_7(OH)_6(H_2O)_6(PW_9O_{34})_2]^{9-}$ (**2**), $[Co_7(OH)_6(H_2O)_4(PW_9O_{34})_2]_n^{9n-}$ (**3**), and $[Co_7(OH)_6(H_2O)_6(P_2W_{15}O_{62})_2]^{15-}$ (**4**).

POM $[Co_7(OH)_6(H_2O)_2(CH_3COO)_4(PW_9O_{34})_2]^{13-}$ (**1**), reported for the first time in this work, has been obtained following the first type of approach (see the experimental section for the details). Interestingly, we have found that POM **1** can also be obtained (although with a much lower yield) following the synthetic procedure to obtain the related POM **2** [21] (in which no acetate ligands are present). In that alternative procedure, POM **1** crystallizes from the mother liquor that results when POM **2** is filtered out from the solution. The polyoxoanions of **2** that have not been crystallized remain in solution as the solvent keeps evaporating and the acetate concentration increases, promoting the substitution of the terminal water molecules in **2** by acetate ligands. As the acetate ligands are incorporated into the POM, its anionic charge increases, presumably reducing its solubility. Therefore, the most likely reason for not obtaining a fully substituted compound (with six acetate ligands) is that the partially substituted one reaches its solubility limit before the full substitution takes place in significant amounts.

### *3.2. Crystal Structure*

The polyoxoanion $[Co_7(OH)_6(H_2O)_2(CH_3COO)_4(PW_9O_{34})_2]^{13-}$ (**1**) consists of a heptanuclear cobalt cluster in which the cobalt atoms are coordinated by two heptadentate B-α-$[PW_9O_{34}]^{9-}$ ligands, six $\mu_3$ hydroxyls, and six terminal ligands (four acetate anions and two water molecules), see Figure 2a. The heptanuclear cluster can be topologically described as a $\{Co_7O_8\}$ di-cubane having two chemically different cobalt atoms (see Figure 2b): one central cobalt atom (Co1) at an inversion center (not directly coordinated by the trivacant B-α-$[PW_9O_{34}]^{9-}$ unit) and six cobalt atoms (Co2 and Co3 in the asymmetric

unit) which are arranged in two separated triads, each of them sharing a common oxygen (O3 in Figure 2b) with the phosphorus atom of a trivacant POM unit.

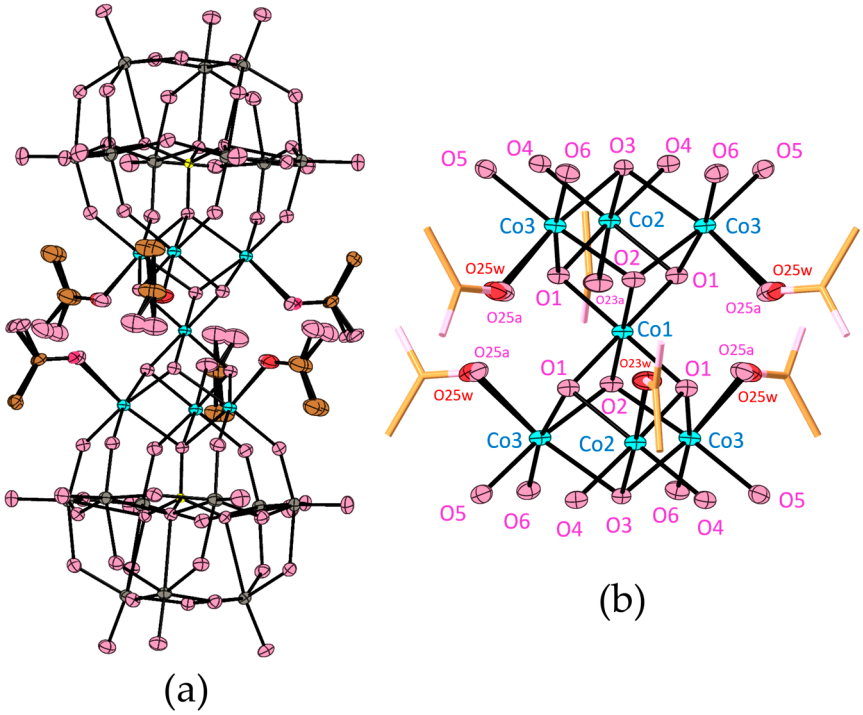


**Figure 2.** (**a**) Ellipsoid representation of POM **1** showing the disorder in the acetate groups and water molecules; (**b**) ellipsoid representation and atom labeling of the heptacobalt dicubane cluster contained in **1**, showing the disorder between the water molecules and acetate groups in the coordinating positions of the six $Co^{2+}$ ions (only one component of the disordered acetate groups is shown). Grey ellipsoids: W; yellow ellipsoids: P; red ellipsoids: O from coordinating water molecules; pink ellipsoids: other O; blue ellipsoids: Co; brown ellipsoids: C; acetate groups in (**a**) are shown as stick representations in (**a**). Hydrogen atoms from methyl groups have been omitted.

BVS calculations [28–30] clearly indicate that Co1 exhibits an oxidation state of +3, while all other cobalt atoms are divalent. In addition, BVS calculations confirm that the six $\mu_3$-O ligands (O1 and O2 in the asymmetric unit) that coordinate the $Co^{3+}$ ion and two $Co^{2+}$ ions correspond to hydroxyl groups. Therefore, each of the six $Co^{2+}$ ions is coordinated by three oxygen atoms belonging to a B-α-$[PW_9O_{34}]^{9-}$ trivacant unit, two hydroxyl groups, and one terminal ligand (water or acetate) that completes the octahedral coordination. The four acetate anions (acting as unidentate ligands) and the two water molecules are statistically disordered on the six positions that coordinate the six $Co^{2+}$ ions. We previously reported the synthesis and characterization of $[Co_7(OH)_6(H_2O)_6(PW_9O_{34})_2]^{9-}$ (**2**) and $[Co_7(OH)_6(H_2O)_4(PW_9O_{34})_2]_n^{9n-}$ (**3**), both containing the same $\{Co_7O_8\}$ dicubane cluster as **1**, but **2** has six water molecules (and no acetate ligands) coordinating the six $Co^{2+}$ ions [21], while in **3** two aquo ligands have been substituted by oxygen atoms of neighboring POMs, giving rise to a polymeric chain of polyoxoanions [21]. All Co–O distances in **1**, **2,** and **3** are very similar (see Table 2), suggesting that the substitution of four of the six water molecules in **2** to give rise to **1** has a negligible effect on the geometry of the heptanuclear cobalt cluster. Only a slight difference can be appreciated in the Co–O (terminal) bond distances when water molecules are substituted by acetate ligands: As expected, the charged acetate ligands are slightly closer to the $Co^{2+}$ ions (2.043(18) and 2.07(3) in (**1**)) than the water molecules (2.17(4) and 2.16(5) in **1**, and 2.13(3)–2.21(3) in **2**).

**Table 2.** Co–O bond distances (Å) involved in the heptanuclear dicubane cluster contained in POM **1** (atom labels are shown in Figure 2b), and ranges of the same distances in POMs **2** and **3**. The Co–O distances are classified according to the different types of oxygen atoms: $O^H$ (hydroxyl oxygen), $O^P$ (oxygen bonded to phosphorus), $O^W$ (oxygen bonded to tungsten), $O^{2H}$ (water oxygen), and $O^{Ac}$ (acetate oxygen).

| Type of Distance | **1** [1] | **2** | **3** |
|---|---|---|---|
| Co(III)–$O^H$ | Co1–O1 1.927(3) × 4<br>Co1–O2 1.919(5) × 2 | 1.91(3)–1.93(3) | 1.912(11)–1.917(12) |
| Co(II)–$O^H$ | Co2–O1 2.091(3) × 4<br>Co3–O1 2.092(3) × 4<br>Co3–O2 2.090(3) × 4 | 2.06(3)–2.11(3) | 2.069(10)–2.096(11) |
| Co(II)–$O^P$ | Co2–O3 2.282(4) × 2<br>Co3–O3 2.273(3) × 4 | 2.24(2)–2.29(2) | 2.232(10)–2.263(10) |
| Co(II)–$O^W$ | Co2–O4 2.038(3) × 4<br>Co3–O5 2.026(4) × 4<br>Co3–O6 2.034(3) × 4 | 1.97(3)–2.09(3) | 1.984(11)–2.030(11) |
| Co(II)–$O^{2H}$ | Co2–$O23_{water}$ 2.17(4) × 2<br>Co3–$O25_{water}$ 2.16(5) × 4 | 2.13(3)–2.21(3) | 2.100(10)–2.163(11) |
| Co(II)–$O^{Ac}$ | Co2–O23a 2.043(18) × 2<br>Co3–O25a 2.07(3) × 4 | — | — |

[1] The multiplier indicates the number of times that a particular distance appears in the dicubane cluster.

### *3.3. IR Spectroscopy, TGA-DTA, UV-Vis-NIR Diffuse Reflectance Spectroscopy, and PXRD*

The IR spectra of POMs **1** and **2** in the fingerprint region are displayed together in Figure 3 for comparison. The IR bands attributed to the polyoxometalate skeleton [31] are very similar in both compounds (in $cm^{-1}$): P-O bands are at 1025s for **1** and **2**; W-O (terminal) at 950sh and 927s for **1**, and at 949sh and 928s for **2**; W-O-W (corner-sharing $WO_6$ octahedra) at 868s for **1**, and at 867s for **2**; W-O-W (edge-sharing octahedra) at 791s and 705s for **1**, and at 792 and 707 for **2**. The IR spectrum of **1** exhibits additional bands that can be attributed to the acetate ligands [32]: 1540m ($\nu_8$, $CO_2$ asym. stretching), 1410m ($\nu_2$, $CO_2$ sym. stretching), 1350sh ($\nu_3$, $CH_3$ sym. bending), 1054m ($\nu_{14}$, $CH_3$ rocking), and 662w ($\nu_5$, $CO_2$ sym. bending). The IR bands can be used to distinguish between different coordination modes of the acetate ligand in metal complexes [32], according to the following ranges of the difference $\Delta = \nu_8 - \nu_2$: 105–140 $cm^{-1}$ for monodentate bonding, 145–185 $cm^{-1}$ for bidentate chelate bonding, and 180–190 $cm^{-1}$ for bidentate bridging bonding. Applying these to the IR spectrum of **1**, we obtain 1540 − 1410 = 130 $cm^{-1}$, which clearly associates the acetate ligands in **1** with monodentate bonding, in agreement with the crystal structure of **1**.

The TGA–DTA curves of $Na_{13}$-**1**·$37H_2O$ are shown in Figure 4. The TGA curve suggests that a partial dehydration process takes place between 30 and 100 °C, with a mass loss of 9.15%, corresponding to the evolution of 32 water molecules (calcd. 9.28%). The slight slope change observed at 40 °C could indicate a different rate of release of water molecules. Two exothermic peaks in the DTA curve, at 37 and 73 °C, presumably correspond to different solvation water molecules. A gradual mass loss takes place from 100 to 353 °C, where an abrupt mass loss starts, finishing at 382 °C. The observed total mass loss between 100 and 382 °C is 6.21%, which can be related to the loss of the remaining seven (coordinated and uncoordinated) water molecules and four acetate ligands (calcd. 5.83%). The exothermic peak in the DTA curve at 381 °C can be attributed to the oxidative degradation of the acetate ligands. At higher temperatures, the collapse of the POM framework must take place. Cobalt may end as a mixture of different cobalt oxides (e.g.,

CoO, $Co_3O_4$, or $Co_2O_3$) or, when tungsten is present, even $CoWO_4$ [33]. If, for simplicity, we assume that the final decomposition product contains only $CoWO_4$, $WO_3$, $Na_2O$, and $P_2O_5$, the total calculated mass loss is 15.60%, while the experimental loss at 678 °C is 16.19%.

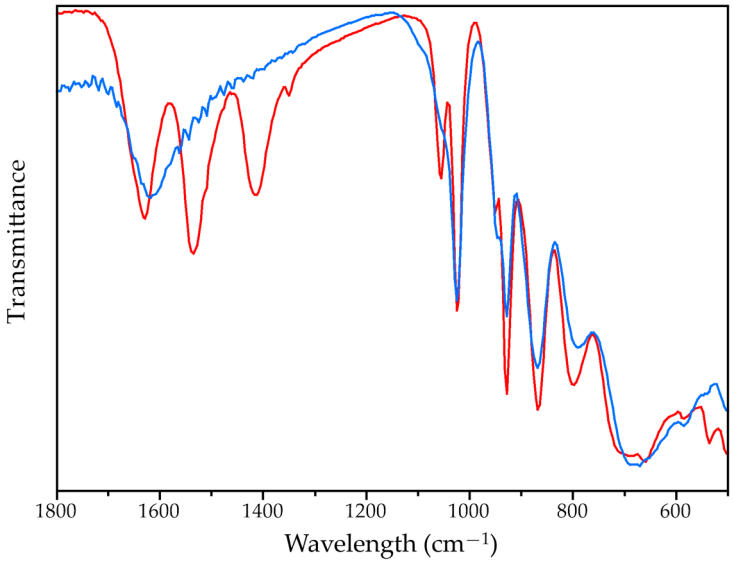


**Figure 3.** FTIR spectra of the salts of POMs **1** (red line) and **2** (blue line).

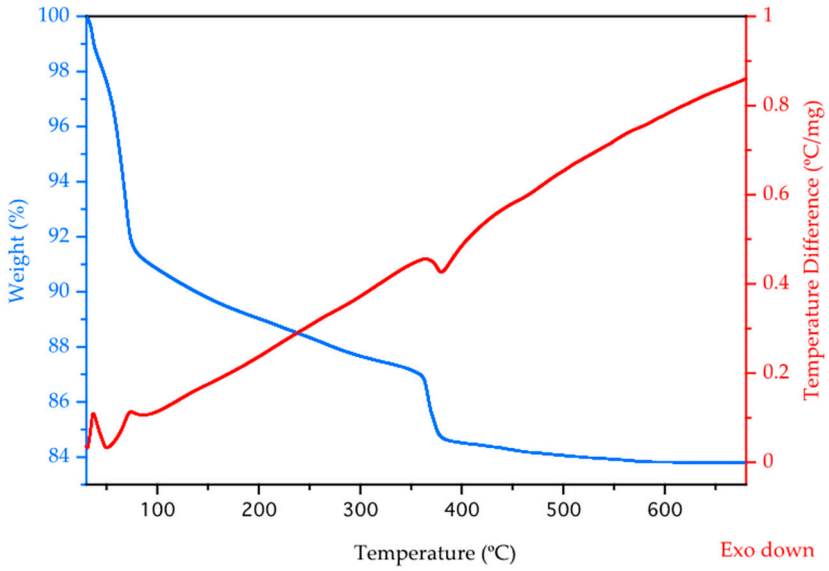


**Figure 4.** TGA–TDA curves of $Na_{13}$-**1**·$37H_2O$ (blue and red, respectively).

The solid UV-Vis-NIR spectrum of $Na_{13}$-**1**·$37H_2O$ is displayed in Figure S3. The strong absorption in the higher energy region ($\lambda < 250$ nm), tailing well into the visible, can be attributed to ligand-to-metal (LMCT) $O_{2p} \rightarrow W_{5p}$ charge transfer electronic transitions, common to all polyoxotungstates [34]. The band in the visible region, having a maximum at 543 nm, is very similar to the bands of monosubstituted Co(II) Keggin polyoxoanions and, therefore, can be ascribed to the octahedral Co(II) d–d electronic transition $^4T_{1g}$ (P) $\leftarrow$ $^4T_{1g}$ (F) [35]. The splitting of this transition to $^4T_{1g}$ (P) has been attributed to spin–orbit coupling.

The experimental PXRD pattern of a bulk sample of $Na_{13}$-**1**·$37H_2O$ (see Figure S2) shows a very good agreement with the simulated pattern generated from the atomic coordinates of the single-crystal structure solution, although with some preferred orientation effects resulting from the high crystallinity of the material.

### *3.4. Magnetic Properties*

The magnetic susceptibility on a ground polycrystalline sample of $Na_{13}$-**1**·$37H_2O$ is shown in Figure 5 as a plot of $\chi_m T$ vs. $T$, and Figure 6 shows a plot of the isothermal magnetization vs. H measured from 0 to 5 T at 2 and 5 K. The $\chi_m T$ vs. $T$ curves exhibit a smooth and continuous decrease from room temperature ($\chi_m T$ = 25.8 emuKmol$^{-1}$), and a more abrupt decrease below 20 K, indicating strong antiferromagnetic interactions within the heptacobalt units. This continuous decrease in the $\chi_m T$ value is due to the spin–orbit coupling of the $Co^{2+}$ ions. High-spin octahedral $Co^{2+}$ is an orbitally degenerate ion with a $^4T_1$ ground electronic term. Due to spin–orbit coupling and the low-symmetry crystal field, this ground term splits into six Kramers doublets. The smooth decrease from room temperature in all measurements can be attributed to the depopulation of the higher Kramers doublets. At lower temperatures (below 30 K), only the lowest Kramers doublet is significantly populated so that the exchange interaction between two octahedral $Co^{2+}$ ions can be conveniently described by assuming a coupling between these fully anisotropic Kramers doublets with effective spins ½.

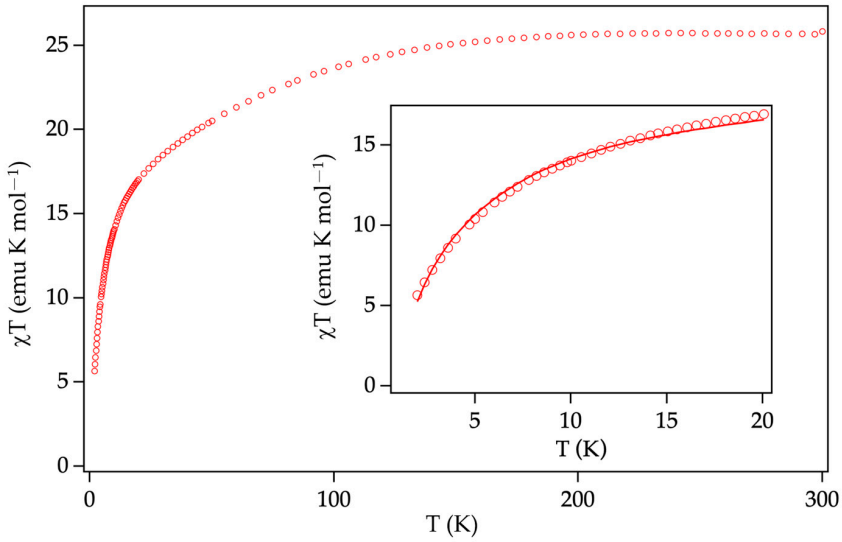


**Figure 5.** Experimental $\chi_M T$ of the heptanuclear cluster in POM **1** at 0.1 T in the range 2–300 K. Inset: Thermal behavior of $\chi_M T$ at 0.1 T in the range 2–20 K, and the solid line represents the theoretical simulation from the best fit.

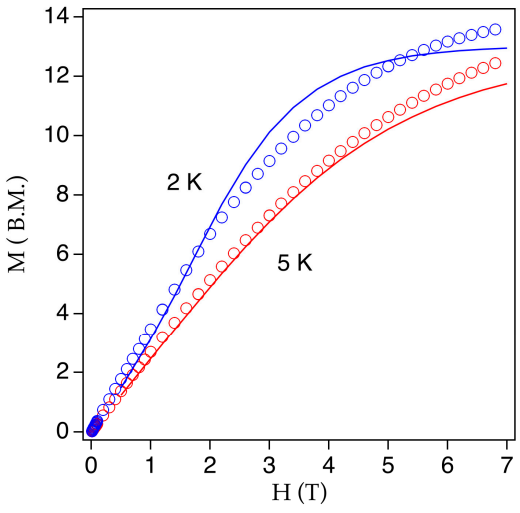


**Figure 6.** Experimental magnetization of the heptanuclear cluster in POM **1** at 2 and 5 K in the range 0–7 T. Solid lines represent the theoretical simulation from the best fit.

The Co-O distances for the central cobalt atom of the heptacobalt cluster are typical of the oxidation state +3. As already described for the other POMs containing these dicubane units [21], this central cobalt should be diamagnetic due to the strong field associated with the hydroxyl groups and only plays the role of an exchange pathway between the other spins. Typically, magnetic interactions between paramagnetic sites through diamagnetic metal ions are negligible or weakly antiferromagnetic.

Taking into account all aspects mentioned above, the effective exchange Hamiltonian for compound $Na_{13}$-**1**·$37H_2O$ can be written as Equation (1):

$$\hat{H} = -2\sum_{i=x,y,z}\{J_i(\hat{S}_i^1\hat{S}_i^2 + \hat{S}_i^1\hat{S}_i^3 + \hat{S}_i^2\hat{S}_i^3 + \hat{S}_i^4\hat{S}_i^5 + \hat{S}_i^4\hat{S}_i^6 + \hat{S}_i^5\hat{S}_i^6) + 2J'(\hat{S}^1 + \hat{S}^2 + \hat{S}^3)(\hat{S}^4 + \hat{S}^5 + \hat{S}^6)\} \quad (1)$$

where $J_i$ represents the exchange components associated with the pathway between the three magnetically equivalent cobalt ions on each trinuclear unit. On the other hand, $J'$ is associated with the exchange interaction between cobalt ions from different trinuclear units through the diamagnetic central $Co^{3+}$. In order to simplify the number of parameters, an axial coupling has been considered between the cobalt ions inside each trinuclear unit ($J_x = J_y$), and the inter-trinuclear interaction has been considered isotropic and equal between all of them. Due to the disorder of the acetate groups and water molecules on the terminal coordinating positions, these parameters will correspond to an average value of interactions. A fit of the susceptibility times temperature product at 0.1 T was performed by numerical diagonalization of the full eigenmatrix, giving the following sets of parameters: $J_x = J_y = 6.2\ cm^{-1}$, $J_z = 14.8\ cm^{-1}$, $J' = -0.226\ cm^{-1}$, $g_{av} = 4.40$ ($R = 3.6 \times 10^{-4}$. Other fits of similar quality can be obtained with $J_z/J_{xy}$ ratios closer to 1. This indicates that the fit is not very sensitive to the anisotropy of this interaction. In fact, when the magnetization adjustment is introduced, the best solution is obtained with an almost isotropic $J$ with a value of $11.6\ cm^{-1}$. At low temperature, where the antiferromagnetic interaction between the two trimeric units is dominant and the effective spin 1/2 model is valid, much of the sensitivity to the anisotropy is lost. For this reason, different $J_z/J_{xy}$ ratios can be obtained with adjustments of similar quality. It should be noted that the average value of this interaction ($9.05\ cm^{-1}$) is very similar to the rest of the heptameric systems [21] and other previously studied cobalt systems [19]. This is also so because the presence of the acetate groups does not considerably alter the Co–O–Co angles.

## 4. Conclusions

In this work, we have described the synthesis of a new member of a series of POM compounds ($[Co_7(OH)_6(H_2O)_2(CH_3COO)_4(PW_9O_{34})_2]^{13-}$ (**1**)), in which two heptadentate lacunary POM ligands encapsulate a heptanuclear cobalt cluster having a dicubane topology. This dicubane cluster contains six $Co^{2+}$ ions and one central $Co^{3+}$ ion coordinated by six $\mu_3$-hydroxyl ligands, which justify the occurrence of this oxidation state in the cluster. Every $Co^{2+}$ ion is coordinated by two of these $\mu_3$-OH groups, three oxo ligands from the lacunary POM units, and one terminal ligand, which can be a water molecule or an acetate anion acting as a monodentate ligand. In the previously reported POM $[Co_7(OH)_6(H_2O)_6(PW_9O_{34})_2]^{9-}$ (**2**), all six terminal ligands were water molecules, while in **1**, four of them have been replaced by acetate groups. The magnetic properties of **1** are interpreted based on an antiferromagnetic coupling between two identical ferromagnetically coupled tricobalt units. A complex level scheme with a diamagnetic ground state (S = 0), quasidegenerate with an antisymmetric combination of ± M functions, is obtained. The substitution of some of the water molecules by acetate ligands in **1** does not significantly affect the geometry of the cluster, and then, the exchange parameters are

similar to those obtained for the previously reported heptameric cobalt clusters having six water molecules as terminal ligands of the $Co^{2+}$ ions [21]. In any case, spectroscopic studies, for example, with inelastic neutron scattering, which determine energy levels directly, can help determine anisotropy. Furthermore, they will allow the use of models that explicitly introduce the orbital contribution and not just consider the fundamental Kramer doublet.

The preparation of **1** suggests that the substitution of the coordinating water molecules by other ligands is relatively easy in this dicubane cluster, allowing the functionalization of this magnetic POM, even with different degrees of ligand substitution. In this sense, an interesting research direction would be the use of dicarboxylate ligands that could allow the connection of the heptanuclear clusters along different directions of space and, then, the formation of MOFs based on POMs (POMOFs).

**Supplementary Materials:** The following supporting information can be downloaded at https://www.mdpi.com/article/10.3390/magnetochemistry11060048/s1, Table S1: O–Co–O angles in the heptanuclear cluster of $Na_{13}[Co_7(OH)_6(H_2O)_2(CH_3COO)_4(PW_9O_{34})_2]\cdot 37H_2O$ (**1**); Figure S1: Representation and atom labeling of the heptanuclear cluster in **1**; Table S2: Valence bond sum calculations for selected atoms in **1**; Figure S2: Powder X-ray diffraction pattern of **1**; Figure S3: UV-vis-NIR diffuse reflectance spectrum of $Na_{13}$-**1**$\cdot 37H_2O$; Figure S4: Additional crystal structure images of **1**. See Refs. [28–30].

**Author Contributions:** Conceptualization, C.G.-S.; methodology, C.G.-S. and J.M.C.-J.; software, J.M.C.-J.; validation, G.A.-D.; formal analysis, C.G.-S., J.M.C.-J., and G.A.-D.; investigation, C.G.-S., J.M.C.-J., and G.A.-D.; resources, C.G.-S.; data curation, C.G.-S., J.M.C.-J., and G.A.-D.; writing—original draft preparation, C.G.-S. and J.M.C.-J.; writing—review and editing, C.G.-S. and J.M.C.-J.; visualization, C.G.-S., J.M.C.-J., and G.A.-D.; supervision, C.G.-S.; project administration, J.M.C.-J. and C.G.-S.; funding acquisition, J.M.C.-J. and C.G.-S. All authors have read and agreed to the published version of the manuscript.

**Funding:** This study forms part of the Advanced Materials program and was supported by the Spanish MCIN with funding from European Union NextGeneration EU (PRTR-C17.I1), the Spanish MICIN grant (No. PID2020-117177GB-I00), and the Generalitat Valenciana (project MFA-2022-057). We also thank the project CIPROM-2022-060 from the Generalitat Valenciana for financial support. This project was also developed within the framework of the University of Valencia Vice-Rector's Office for Research program, call for special actions, reference UV-INV_AE-2667242.

**Institutional Review Board Statement:** Not applicable.

**Informed Consent Statement:** Not applicable.

**Data Availability Statement:** The original contributions presented in this study are included in the article/Supplementary Materials. Further inquiries can be directed to the corresponding authors.

**Acknowledgments:** We acknowledge J. M. Martínez-Agudo for technical support.

**Conflicts of Interest:** The authors declare no conflicts of interest.

## Abbreviations

The following abbreviations are used in this manuscript:

| | |
|---|---|
| ATR | Attenuated total reflectance |
| BVS | Bond valence sum |
| CCD | Charge-coupled device |
| DTA | Differential thermal analysis |
| EDX | Energy-dispersive X-ray spectroscopy |
| FTIR | Fourier transform infrared spectroscopy |
| IR | Infrared |
| POM | Polyoxometalate |

| | |
|---|---|
| PXRD | Powder X-ray diffraction |
| TGA | Thermogravimetric analysis |
| UV-Vis-NIR | Ultraviolet–visible–near infrared |

## References


1. Pope, M.T. *Heteropoly and Isopoly Oxometalates*; Springer: New York, NY, USA; Berlin/Heidelberg, Germany; Tokyo, Japan, 1983; ISBN 0387118896.
2. Pope, M.T.; Müller, A. Polyoxometalate Chemistry: An Old Field with New Dimensions in Several Disciplines. *Angew. Chem. Int. Ed. Engl.* **1991**, *30*, 34–48. [CrossRef]
3. Iftikhar, T.; Rosnes, M.H. Covalent Organic-Inorganic Polyoxometalate Hybrids in Catalysis. *Front. Chem.* **2024**, *12*, 1447623. [CrossRef]
4. Sun, Z.; Wang, R.; Kozhevnikov, I.V. Versatile POMOF-Based Materials: Synthesis, Mechanism, Topology and Catalytic Applications. *Coord. Chem. Rev.* **2025**, *524*, 216304. [CrossRef]
5. Gumerova, N.I.; Rompel, A. Synthesis, Structures and Applications of Electron-Rich Polyoxometalates. *Nat. Rev. Chem.* **2018**, *2*, 0112. [CrossRef]
6. Absalan, Y.; Gholizadeh, M.; Kim, E.-B.; Ameen, S.; Wang, Y.; Wang, Y.; He, H. Recent Progress on Organic Metal Compound/MOF Hybrids: From Controllable Synthesis to Potential Catalytic Applications. *Coord. Chem. Rev.* **2024**, *515*, 215972. [CrossRef]
7. Ren, Y.; Wang, M.; Chen, X.; Yue, B.; He, H. Heterogeneous Catalysis of Polyoxometalate Based Organic-Inorganic Hybrids. *Materials* **2015**, *8*, 1545–1567. [CrossRef] [PubMed]
8. Ma, M.; Chen, J.; Dong, L.; Su, Y.; Tian, S.; Zhou, Y.; Li, M. Polyoxometalates and Their Composites for Antimicrobial Applications: Advances, Mechanisms and Future Prospects. *J. Inorg. Biochem.* **2025**, *262*, 112739. [CrossRef]
9. Liu, J.; Huang, M.; Zhang, X.; Hua, Z.; Feng, Z.; Dong, Y.; Sun, T.; Sun, X.; Chen, C. Polyoxometalate Nanomaterials for Enhanced Reactive Oxygen Species Theranostics. *Coord. Chem. Rev.* **2022**, *472*, 214785. [CrossRef]
10. Hu, Y.; Wang, Y.; Zhao, J.; Chen, L. Recent Advances of Polyoxometalate-Based Materials Applied for Electron-Related Devices. *Coord. Chem. Rev.* **2024**, *506*, 215724. [CrossRef]
11. Kruse, J.-H.; Langer, M.; Romanenko, I.; Trentin, I.; Hernandez-Castillo, D.; Gonzalez, L.; Schacher, F.H.; Streb, C. Polyoxometalate-Soft Matter Composite Materials: Design Strategies, Applications, and Future Directions. *Adv. Funct. Mater.* **2022**, *32*, 2208428. [CrossRef]
12. Verissimo, M.I.S.; Evtuguin, D.V.; Gomes, M.T.S.R. Polyoxometalate Functionalized Sensors: A Review. *Front. Chem.* **2022**, *10*, 840657. [CrossRef] [PubMed]
13. Housaindokht, M.R.; Jamshidi, A.; Janati-Fard, F. Recent Advances in Polyoxometalates for Spectroscopic Sensors: A Review. *J. Mater. Sci.* **2022**, *57*, 13871–13902. [CrossRef]
14. Clemente-Juan, J.M.; Coronado, E.; Gaita-Arino, A. Magnetic Polyoxometalates: From Molecular Magnetism to Molecular Spintronics and Quantum Computing. *Chem. Soc. Rev.* **2012**, *41*, 7464–7478. [CrossRef]
15. Yang, Z.-X.; Gong, F.; Lin, D.; Huo, Y. Recent Advances in Polyoxometalate-Based Single-Molecule Magnets. *Coord. Chem. Rev.* **2023**, *492*, 215205. [CrossRef]
16. Baldoví, J.J.; Cardona-Serra, S.; Gaita-Ariño, A.; Coronado, E. Design of Magnetic Polyoxometalates for Molecular Spintronics and as Spin Qubits. In *Advances in Inorganic Chemistry, Vol 69: Polyoxometalate Chemistry*; VanEldik, R., Cronin, L., Eds.; Univ Valencia, Inst Ciencia Mol ICMol: Paterna, Spain, 2017; Volume 69, pp. 213–249. ISBN 0898-8838.
17. Tsukerblat, B.; Palii, A.; Clemente-Juan, J.M.; Gaita-Arino, A.; Coronado, E. A Symmetry Adapted Approach to the Dynamic Jahn-Teller Problem: Application to Mixed-Valence Polyoxometalate Clusters with Keggin Structure. *Int. J. Quantum Chem.* **2012**, *112*, 2957–2964. [CrossRef]
18. Palii, A.; Tsukerblat, B.; Klokishner, S.; Dunbar, K.R.; Clemente-Juan, J.M.; Coronado, E. Beyond the Spin Model: Exchange Coupling in Molecular Magnets with Unquenched Orbital Angular Momenta. *Chem. Soc. Rev.* **2011**, *40*, 3130–3156. [CrossRef]
19. Clemente-Juan, J.M.; Coronado, E.; Gaita-Ariño, A.; Giménez-Saiz, C.; Güdel, H.-U.; Sieber, A.; Bircher, R.; Mutka, H. Magnetic Polyoxometalates: Anisotropic Exchange Interactions in the $Co_3^{II}$ Moiety of $[(NaOH_2)Co_3(H_2O)(P_2W_{15}O_{56})_2]^{17-}$. *Inorg. Chem.* **2005**, *44*, 3389–3395. [CrossRef]
20. Galán-Mascarós, J.R.; Gómez-Garcia, C.J.; Borrás-Almenar, J.J.; Coronado, E. High Nuclearity Magnetic Clusters: Magnetic Properties of a Nine Cobalt Cluster Encapsulated in a Polyoxometalate, $[Co_9(OH)_3(H_2O)_6(HPO_4)_2(PW_9O_{34})_3]^{16-}$. *Adv. Mater.* **1994**, *6*, 221–223. [CrossRef]
21. Duan, Y.; Clemente-Juan, J.M.; Giménez-Saiz, C.; Coronado, E. Cobalt Clusters with Cubane-Type Topologies Based on Trivacant Polyoxometalate Ligands. *Inorg. Chem.* **2016**, *55*, 925–938. [CrossRef]
22. Bassil, B.S.; Xiang, Y.; Haider, A.; Hurtado, J.; Novitchi, G.; Powell, A.K.; Bossoh, A.M.; Mbomekallé, I.M.; de Oliveira, P.; Kortz, U. Heptanickel(II) Double-Cubane Core in Wells-Dawson Heteropolytungstate, $[Ni_7(OH)_6(H_2O)_6(P_2W_{15}O_{56})_2]^{16-}$. *Chem. Commun.* **2016**, *52*, 2601–2604. [CrossRef]

23. Zhang, Z.; Wang, E.; Qi, Y.; Li, Y.; Mao, B.; Su, Z. Synthesis, Characterization, and Crystal Structures of Double-Cubane-Substituted and Asymmetric Penta-Ni-Substituted Dimeric Polyoxometalates. *Cryst. Growth Des.* **2007**, *7*, 1305–1311. [CrossRef]
24. Fang, X.; Kögerler, P.; Speldrich, M.; Schilder, H.; Luban, M. A Polyoxometalate-Based Single-Molecule Magnet with an S = 21/2 Ground State. *Chem. Commun.* **2012**, *48*, 1218–1220. [CrossRef] [PubMed]
25. *APEX3*, version v2017.3-0; Bruker AXS Apex3 Inc.: Madison, WI, USA, 2017.
26. Sheldrick, G.M. Crystal Structure Refinement with SHELXL. *Acta Crystallogr. Sect. C Struct. Chem.* **2015**, *71*, 3–8. [CrossRef] [PubMed]
27. Domaille, P.J.; Hervé, G.; Tézé, A. Vanadium(V) Substituted Dodecatungstophosphates. In *Inorganic Syntheses, Volume 27*; Ginsberg, A.P., Ed.; Wiley: Hoboken, NJ, USA, 1990; pp. 96–104.
28. Brown, I.D.; Altermatt, D. Bond-Valence Parameters Obtained from a Systematic Analysis of the Inorganic Crystal Structure Database. *Acta Crystallogr. Sect. B Struct. Sci.* **1985**, *41*, 244–247. [CrossRef]
29. Wood, R.M.; Palenik, G.J. Bond Valence Sums in Coordination Chemistry. A Simple Method for Calculating the Oxidation State of Cobalt in Complexes Containing Only Co−O Bonds. *Inorg. Chem.* **1998**, *37*, 4149–4151. [CrossRef]
30. Brese, N.E.; O'Keeffe, M. Bond-Valence Parameters for Solids. *Acta Crystallogr. Sect. B Struct. Sci.* **1991**, *47*, 192–197. [CrossRef]
31. Finke, R.G.; Droege, M.W.; Domaille, P.J. Trivacant Heteropolytungstate Derivatives. 3. Rational Syntheses, Characterization, Two-Dimensional Tungsten-183 NMR, and Properties of Tungstometallophosphates $P_2W_{18}M_4(H_2O)_2O_{68}^{10-}$ and $P_4W_{30}M_4(H_2O)_2O_{112}^{16-}$ (M = Cobalt, Copper, Zinc). *Inorg. Chem.* **1987**, *26*, 3886–3896. [CrossRef]
32. Nickolov, Z.; Georgiev, G.; Stoilova, D.; Ivanov, I. Raman and IR Study of Cobalt Acetate Dihydrate. *J. Mol. Struct.* **1995**, *354*, 119–125. [CrossRef]
33. Zhang, Z.; Muhammed, M. Thermochemical Decomposition of Cobalt Doped Ammonium Paratungstate Precursor. *Thermochim. Acta* **2003**, *400*, 235–245. [CrossRef]
34. Yamase, T. Photo- and Electrochromism of Polyoxometalates and Related Materials. *Chem. Rev.* **1998**, *98*, 307–326. [CrossRef]
35. Weakley, T.J.R.; Malik, S.A. Heteropolyanions Containing Two Different Heteroatoms—I. *J. Inorg. Nucl. Chem.* **1967**, *29*, 2935–2944. [CrossRef]


**Disclaimer/Publisher's Note:** The statements, opinions and data contained in all publications are solely those of the individual author(s) and contributor(s) and not of MDPI and/or the editor(s). MDPI and/or the editor(s) disclaim responsibility for any injury to people or property resulting from any ideas, methods, instructions or products referred to in the content.